Journal of Robotics and Control (JRC)
Volume 6, Issue 3, 2025
ISSN: 2715-5072, DOI: 10.18196/jrc.v6i3.25992

Enhanced Adaptive Neuro Sliding Mode Controller Parameter Optimization for Coupled Tank System

Nguyen Anh Tuan [1], Ho Pham Huy Anh [2*]
[1] Faculty of Engineering and Technology (FET), Sai Gon University (SGU), 273 An Duong Vuong Street, Ward 2, District 5, Ho Chi Minh City, Viet Nam
[2] Ho Chi Minh City University of Technology (HCMUT), 268 Ly Thuong Kiet Street, District 10, Ho Chi Minh City, Viet Nam
[2] Vietnam National University Ho Chi Minh City (VNU-HCM), Linh Trung Ward, Thu Duc District, Ho Chi Minh City, Viet Nam
Email: [1] nguyenanhtuan.sdh21@hcmut.edu.vn, [2] hphanh@hcmut.edu.vn
Corresponding Author

***Abstract*—This paper proposes the EANSMC-MDE method for the coupled tank system (CTS) liquid level control, which consists of the Improved Difference Evolution (MDE) optimizing method optimized parameters for the Adaptive Neuro Sliding Mode Controller (ANSMC). The CTS system represents a nonlinear object with delay and uncertainties, including varying parameters, sensor and output valve noises, etc. The suggested controller contains a direct adaptive controller directly approximated by a Radial Basis Function (RBF) neural network combined with a sliding mode controller used to compensate for the approximation errors of the RBF network and ensure system stability. The stability Lyapunov criterion is used to construct the sliding-mode control system and adaptive rule. The proposed algorithm delivers good control performance right from the start-up phase thanks to the use of pre-optimized parameters, which is an advantage compared to conventional adaptive control algorithms. Simulations are conducted to demonstrate the effectiveness of the proposed optimization method compared to different optimization methods using identical beginning conditions and objective function values to establish equitable comparisons. Furthermore, to demonstrate the superiority of the suggested control method, it is contrasted with the optimal SMC and the traditional ANSMC method. Additionally, the simulations evaluate the response capability of the proposed algorithm under the influence of significantly varying sensor noise levels across different magnitudes, changes in the reference signal, and substantial variations in system parameters. The proposed algorithm has the potential to be applied to other uncertain nonlinear systems. However, it has not yet been validated on systems with fast dynamic responses.**

Keywords—Improved Difference Evolution (MDE) Method; Adaptive Neuro Sliding Mode Control (ANSMC); Coupled Tank System (CTS); Radial Basis Function Neural Network (RBFNN); Nonlinear Control; System Stability; Optimization Algorithm.

I. INTRODUCTION

The liquid level of tank systems in production plants needs to be precisely controlled as it directly affects the quality of the products, especially in industries like chemicals, oil and gas, food production, etc. Most tank systems are highly nonlinear and have complex uncertainties that change during operation, such as interactions between tanks, delays between input and output, sensor noise, parameter variations during operation, etc. To validate control methods for these tank systems, the coupled-tank system (CTS) is utilized as a representative model. As a result, a variety of control methods, from simple to complex, have been used to control this system. First, the paper [1] uses a decentralized PID controller to control the CTS system. The overshoot is reduced by imposing constraints on the maximum closed-loop amplitude ratio of the system, and system stability is ensured by applying the Kharitonov-Hurwitz theorem. Next, the paper [2] uses a decentralized PI/PID controller based on frequency domain analysis for a two-input, two-output coupled tank system. The control algorithm is implemented for the decoupled subsystems by employing a decoupler. In contrast, paper [3] uses an AI-based online self-tuning algorithm to adjust the PID gains to address the issue of parameter variation. Fuzzy control and SMC algorithms provide faster and more stable responses compared to the PID algorithm in controlling the coupled tank system [4]. Therefore, hybrid PID-SMC algorithms were proposed in [5], [6]. Although the SMC algorithm has better capability to handle nonlinear disturbances than the PID algorithm, one of its drawbacks is its dependence on the control system model [7]. In addition, this method is prone to chattering. To overcome these limitations while still leveraging the fast and stable response advantages of the SMC technique under nonlinear disturbances, the algorithm is improved or integrated with other control strategies.

First, the paper [8] uses a Model-Free Fractional Order Intelligent Proportional Integral-Fractional Order Sliding Mode Controller to address the issues of overshoot and external disturbance in controlling the CTS system. The paper [9] proposes a higher-order sliding mode robust control method for controlling the quadruple tank system. The unmeasurable states are estimated using a sliding mode observer. The authors of the paper [10] propose a novel convergence algorithm for discrete-time systems applied to the CTS system, enabling the system to reach convergence within a user-defined settling time. While paper [11] applies an optimal prescribed-time stabilization method for nonlinear dynamical systems, specifically for the CTS system. The stability and convergence of the system satisfy the Hamilton-Jacobi-Bellman equation and Lyapunov stability theory. The studies [12]-[15] employed a Disturbance Observer to address the issue of external disturbances in the control of CTS and Quadruple-Tank systems. Subsequently, the study

[16] utilized a compensator based on the Bernstein polynomial to mitigate the adverse effects of saturation nonlinearity in process control applications within the CTS system control. However, the issue of how to reduce the impact of external disturbances still needs to be further addressed. Intelligent control solutions have been widely applied to handle increasingly nonlinear systems. Next, the authors in [17] use a Fuzzy PI controller designed using s- and z-type membership functions to address the uncertain environment in CTS system control, showing improved performance over conventional Fuzzy PI controllers. Paper [18] proposed a novel intelligent fuzzy fractional-order proportional-integral controller. To further improve control performance, numerous studies have coupled neural networks or fuzzy logic with advanced control methods like SMC or adaptive methods. The control of nonlinear systems in practice must cope with nonlinear model uncertainties and complex external disturbances that vary during operation. Many studies have employed optimal or online adaptive algorithms to help the control system respond in real-time to these complicated uncertainties. First, Paper [19] solves the optimal tracking control problem for the underactuated quadrotor system with unknown dynamics via Reinforcement Learning. Next, to enhance the stability of the system, the paper [20] proposed a reinforcement learning algorithm with stability constraints based on the Lyapunov stability theory to train neural network controllers for application in the control of CTS systems. The studies [21]-[22] proposed robust optimal tracking control algorithms via the technique of integral reinforcement learning combined with a neural network-based observer to address issues related to general disturbances and saturating voltages in the control of permanent magnet synchronous motors (PMSMs). Furthermore, H_∞ optimal tracking control algorithms were introduced in [23], [24] to handle input constraints and external disturbances. These optimal control algorithms have demonstrated high effectiveness in controlling real systems with unknown dynamics under external disturbances. However, to reach the optimal state of the controller, a certain convergence time is required during the initial phase for the neural network weights, which may impact control quality in systems that demand stable performance from the startup phase. Additionally, adaptive control algorithms combined with fuzzy logic or neural networks have also shown effective control quality in the presence of external noise and disturbances. The studies [25]-[27] proposed adaptive fuzzy and neural SMC algorithms. First is the adaptive fuzzy SMC controller [25], which tackles the issue of external noises and actuator failures. Subsequently, the study [26] proposes a novel adaptive fuzzy sliding mode control method based on a fully tuned recurrent neural network compensator to estimate the comprehensive uncertainties of a reluctance-motor maglev system. In addition, the study [27] utilized a fuzzy state observer with an adaptive neural network-based compensator to implement a sliding mode control strategy, where the compensator is designed using the adaptive neural network approach. Neural networks are commonly used to approximate internal uncertainties and external disturbances in control systems. However, using neural networks for approximation inevitably results in approximation errors. These errors can lead to system instability or slow convergence. Meanwhile, SMC algorithms can ensure fast convergence and robust stability. Therefore, neural networks are often integrated with SMC algorithms. Paper [28] proposed an adaptive neural-network-based SMC method for switching distributed delay systems, where the neural network functions as an observer-based neural compensator to mitigate the effects of unknown system nonlinearities. Approaches using terminal SMC techniques have been adopted to balance convergence time and chattering phenomena [29]-[31]. In addition, a novel second-order sliding mode control scheme based on neural networks was proposed in [32] to address issues of system uncertainty, external disturbances, and input saturation. The second-order non-singular fast terminal sliding mode controller resolves the singularity problem and chattering, enabling the system to converge within a fixed time. Moreover, to effectively counter uncertain disturbances, terminal SMC has also been combined with Extended State Observer (ESO) techniques [33]-[34]. The issue of control input singularities in SMC algorithms is addressed in [35]. Furthermore, other approaches [36], [37] integrate adaptive techniques to enhance the controller's ability to handle parametric uncertainties and external disturbances. Adaptive control algorithms are increasingly being applied using various methodological approaches. First, paper [38] proposes a nonlinear generalized global sliding mode controller to maximize power extraction from a Photovoltaic system. Next, the study [39] proposed combining SMC and fractional-order neural network methods to address the synchronization issue of fractional-order neural networks. The study [40] used a sliding mode controller and an adaptive neural network to control a nonlinear SISO system with unknown dynamics. The study [41] employed an SMC combined with an adaptive neural controller to approximate the nonlinear characteristics and uncertainties online. Leveraging the memory capability of recurrent neural networks, studies [42]-[45] employed an adaptive neural sliding mode controller designed based on a recurrent neural network to ensure optimal tracking performance. To utilize the powerful estimation capabilities of the RBFNN, many studies have employed it to approximate model uncertainties and external disturbances. Initially, paper [46] proposed a model predictive control method based on an RBF net-type coefficient Multi-Input/Multi-Output Auto-Regressive model with eXogenous input for system modeling in the control of the CTS system. Following this, study [47] combined an adaptive neural SMC algorithm with back-stepping to approximate the nonlinear aerodynamic forces and moments of an aircraft. Meanwhile, the adaptive backstepping terminal sliding mode control leverages a physics-informed neural network [48] to estimate and compensate for system uncertainty accurately. Next, the paper [49] introduced an RBFNN-based adaptive sliding mode controller, in which the RBFNN is used to compensate for friction disturbance torque in an electromechanical actuator system. Paper [50] proposed a trajectory-tracking controller based on fixed-time sliding mode control and an RBFNN observer to handle system uncertainties and enable faster convergence of tracking errors. Similarly, studies [51]-[57] proposed integrating RBFNNs with adaptive neuro-sliding mode controllers to estimate model uncertainties and

external perturbations, thereby facilitating faster convergence of tracking errors. In these approaches, the RBFNN approximates nonlinear model uncertainties and disturbances, while the SMC component compensates for the RBFNN's approximation errors, ensuring system convergence and stability. These adaptive neural sliding mode control strategies demonstrate their effectiveness in managing nonlinear model uncertainties and external disturbances. However, most of the adaptive algorithm's parameters are typically determined through a trial-and-error technique, which results in a significant degree of error in the system response during the initial stage. Calculating and selecting controller parameters for nonlinear systems through trial and error is complex, often time-consuming, and still fails to find optimal parameters in many cases. Therefore, many studies aim to find controller parameters by utilizing meta-heuristic optimizing methods to determine globally optimum parameters, even when the objective function is non-differentiable. Initially, the Particle Swarm Optimization (PSO) algorithm was employed for identification and control in studies [58]-[62]. Next, the GA optimization algorithm [63]-[65] is also applied to identification and control tasks. The improved optimization of the ant colonies method [66] and the tree seed optimization method [67] are used to optimize the PID controller parameters for improved control quality. Most meta-heuristic methods are inspired by natural phenomena or the behavior of animals like fish, insects, planets, etc. Due to their advantages and disadvantages, some methods have succeeded, while others are no longer in use. In 2020, RAO introduced an optimization method focused on simplicity and efficiency [68] without relying on natural phenomena or animal behaviors like the methods mentioned above. The quality of optimization methods is often influenced by the parameters chosen, and the strength of the RAO methods is that they only require common control parameters, such as population size and the number of iterations, without needing method-specific control parameters. Taking advantage of the simplicity yet efficiency of this method, the study [69] applied it to solve the grid dispatch problem's optimization in power flow. The proposed method showed better performance compared to several other optimization methods. Subsequently, the RAO-1 optimization algorithm [70] was applied to address the nonlinear and multimodal problem in parameter identification of photovoltaic models. Based on RAO's approach of seeking simple yet effective optimization methods, the study [71] proposed the Fully Informed Search Method (FISA), an improved method of the RAO method. This study demonstrated that the proposed method achieved better optimization performance than several other optimization methods. Differing from the RAO and FISA methods presented above, the DE method, despite requiring the selection of specific method parameters, remains one of the simplest yet effective meta-heuristic methods from its introduction by R. Storn and K. Price. Studies [72]-[77] have demonstrated the effectiveness of the DE method over other methods in optimizing controllers for complex nonlinear systems. To enhance the convergence capability of the DE algorithm, the MDE algorithm was proposed in [78] by balancing the global and local search abilities to find potential global optimal solutions. In addition, a hybrid technique combining the DE algorithm and the Jaya algorithm [79] was employed for optimal identification of the adaptive neural sliding mode controller using an RBF network, achieving superior control performance compared to other advanced control algorithms in precise motion tracking of the piezoelectric actuator. The DE algorithm serves as a global search scheme, and the Jaya algorithm plays the role of local search exploitation to perform offline identification of the black-box model of the piezoelectric actuator. In general, meta-heuristic optimizing techniques contribute to determining the controller's global optimal parameters

Based on the analysis of the above studies, the general trend in control methods is to address model uncertainties and exogenous disturbances to ensure robust and accurate control. In particular, the adaptive neural SMC method with the RBF neural network allows for good approximation of nonlinear uncertainties, combined with the fast convergence characteristic of the SMC method for nonlinear systems, resulting in improved control quality. However, most current adaptive algorithms are initialized with randomly chosen controller parameters, which carries the risk of system instability. To overcome this limitation and leverage the global optimization capability of the MDE algorithm, this paper proposes an Enhanced Adaptive Neuro Sliding Mode Controller (EANSMC) parameter optimization approach for liquid-level handling in the CTS system, in which the controller parameters are tuned using the MDE technique [78]. The stability of the system is ensured by the EANSMC controller, which is constructed using the Lyapunov stability theorem. Each meta-heuristic optimization algorithm has its strategy for updating the next generation. Therefore, the performance of each algorithm may vary depending on the objective function and the system under consideration. In this study, the update mechanism of the MDE algorithm proves to be the most suitable for the considered objective function applied to the CTS system, compared to other optimization algorithms, including PSO [59], GA [63], RAO 3 [68], and FISA [71]. Consequently, this paper proposes the use of the MDE algorithm for optimizing the parameters of the proposed DANSMC controller. However, the limitation is that the ANSMC controller parameters are optimally tuned offline. Therefore, a model of the system is required for parameter optimization. As a result, when applying the controller to a real system, the system model must first be identified before applying MDE to tune the controller parameters. This paper's key contributions include:

- The ANSMC control system is innovatively built without requiring previous specific system knowledge. It consists of two components: an adaptive control part directly approximated online by the RBF network, with the adaptive law eliminating the approximation errors of the RBFNN. The SMC controller is an additional component that guarantees the system's stable convergence. By using Lyapunov's stability theorem in the design process, the stability of the system is ensured.
- The ANSMC controller's parameters are effectively optimized for handling the CTS system, a difficult, nonlinear, and unpredictable system, using the comparison of advanced meta-heuristic techniques. Based on the average results of 10 runs under identical

initial conditions, including the same initial objective function value. Here, the MDE method was found to deliver the best performance.

- Validation of control performance in the presence of sensor noise, parametric disturbances, and varying reference signals under the physical constraints of the CTS system

This paper is organized into five parts: Section I contains the introduction, and Section II covers the CST presentation and the controller. Next, Section III introduces the suggested method. Section IV shows the simulation results, and Section V concludes the paper.

II. DESCRIPTION OF THE CONTROL SYSTEM

The two-DOF uncertain nonlinear CTS model relying on the Quanser tank model is shown in Fig. 1. This CTS model is a component of the quadruple-tank MIMO system shown in Fig. 2.

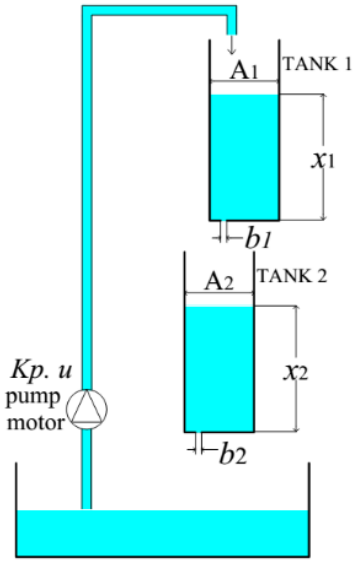

Fig. 1. Coupled tank (CTS) system

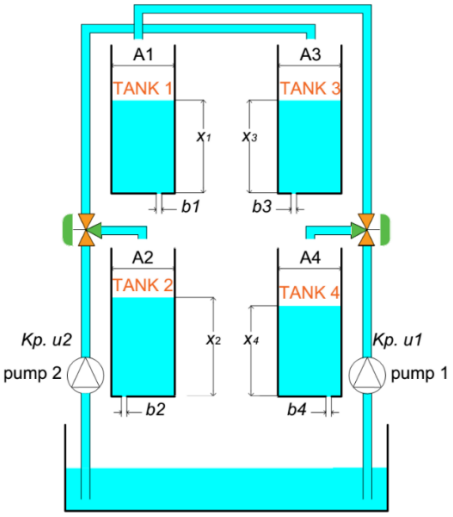

Fig. 2. Quadruple-tank system (QTS)

The CTS system consists of a pump controlled by a voltage u, directly regulating the water flow into Tank 1. Tank 2 receives water from the outlet of Tank 1. The CTS system's mathematical model, presented in [72], is outlined.

$$\begin{cases} \dot{x}_1 = \dfrac{1}{A_1}(K_p u - b_1 C_1 \sqrt{2gx_1}) \\ \dot{x}_2 = \dfrac{1}{A_2}(b_1 C_1 \sqrt{2gx_1} - b_2 C_2 \sqrt{2gx_2}) \end{cases} \quad (1)$$

In Tank 1 and Tank 2, the water levels are represented by x_1, x_2 and u denotes the controlling voltage for the actuator, which is the plant's input. The output of the plant may be either x_1, x_2 or both x_1 and x_2. The task of the control system is to regulate the liquid level in either Tank 1, Tank 2, or both tanks, following a desired signal. This paper focuses on controlling the water level in Tank 2. The physical implications of these characteristics are shown in Table I.

TABLE I. COUPLED-TANK SYSTEM PARAMETERS EMPLOYED FOR BENCHMARK-TEST

Symbol	Explanation	Size	Unit
A_1	Surface area of tank 1's interior	16.619	cm^2
A_2	Surface area of tank 2's interior	16.619	cm^2
b_1	The drainpipe's cross-sectional area in Tank 1	1	cm^2
b_2	The drainpipe's cross-sectional area in Tank 2	1	cm^2
C_1	Tank 1 outlet discharge coefficient	0.8	
C_2	Tank 2 outlet discharge coefficient	0.8	
g	Gravitation force	981	cm/s^2
K_p	Gain of the pump	50	$cm^3/(s.V)$

III. THE PROPOSED EANSMC-MDE CONTROLLER

A. The Problem Statement and ANSMC Controlling Technique

The following content describes the implementation of the ANSMC controller for the CTS plant (2).

$$\begin{cases} \dot{x} = f(x) + g(u) \\ y = h(x) \end{cases} \quad (2)$$

Let $h(x) = x_2$. Then equation (2) can be rewritten as

$$\begin{cases} \dot{x}_1 = \dfrac{1}{A_1}(K_p u - b_1 C_1 \sqrt{2gx_1}) \\ \dot{x}_2 = \dfrac{1}{A_2}(b_1 C_1 \sqrt{2gx_1} - b_2 C_2 \sqrt{2gx_2}) \\ y = x_2 \end{cases} \quad (3)$$

The CST system (2) has two degrees of freedom.

$$\ddot{y} = a(x) + b(x)u \quad (4)$$

Regulating the output $y(t)$ to follow the predetermined required curve $y_d(t)$ It is the duty to solve.

The conventional SMC control law is developed as follows.

Choose $e = y_d - y$, where y_d is the desired reference signal. It follows that

$$\dot{e} = \dot{y}_d - \dot{y}$$

Hence,

$$\ddot{e} = \ddot{y}_d - \ddot{y} = \ddot{y}_d - (a(x) + b(x)u) \quad (5)$$

The CTS system (2) has the second order. Choose the sliding surface as follows.

$$S = \dot{e} + ke \quad (6)$$

Then,

$$\dot{S} = \ddot{e} + k\dot{e} \quad (7)$$

Substituting (5) into (7) yields the following equation.

$$\dot{S} = \ddot{y}_d - (a(x) + b(x)u) + k\dot{e} \quad (8)$$

Choose a quadratic Lyapunov function.

$$V_1 = \frac{1}{2}S^2 \quad (9)$$

Then,

$$\dot{V}_1 = S\dot{S} \quad (10)$$

Choose the derivative of the sliding surface as follows.

$$\dot{S} = -Ksign(S) \quad (11)$$

Where *K* is a positive constant. It follows that

$$\dot{V}_1 = -K|S| \leq 0 \quad (12)$$

Substituting (8) into (11) gives the SMC law as follows.

$$u = \frac{1}{b(x)}[-a(x) + \ddot{y}_d + k\dot{e} + Ksign(S)] \quad (13)$$

Where, *k* is selected to satisfy the Routh-Hurwitz criteria.

The quadratic Lyapunov function (9) satisfies $\dot{V}_1 \leq 0$ as shown in (12). Therefore, the system is stable according to Lyapunov's stability criterion.

The sliding control law (13) can be rewritten as follows.

$$u = \frac{1}{b(x)}[-a(x) + v(t)] \quad (14)$$

Problem 1 formulation:

In this case, *v*(*t*) denotes the system's input signal. Therefore, the linearized feedback law can be used to generate the controller (14) if both the nonlinear functions $a(x)$ and $b(x)$ are known beforehand. Nevertheless, in many real-world situations, the descriptions $a(x)$, $b(x)$ are either undetermined or altered while in operating mode. Suppose these two components are unknown; the control law (14) cannot be implemented in this case. Therefore, the problem is to design a control law that allows for online estimation of the nonlinear elements $a(x)$, $b(x)$ and thus calculate the controller *u*. This rule is referred to as indirect adaptive control. If the control law *u* is estimated directly, it is known as direct adaptive control. To address this issue, this research suggests a direct adaptive sliding mode controller, which is shown in Fig. 3.

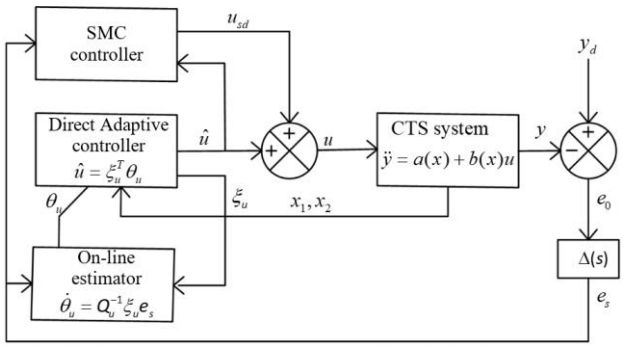

Fig. 3. Layout of the CTS plant's ANSMC controller

The suggested ANSMC for the doubled-tank plant is shown in Fig. 3. The ANSMC control law (22) consists of two components: the adaptive control component $\hat{u}$ (15) and the sliding control component u_{sd} (37), which are computed based on the system state *x*, the sliding surface e_s (25), and the output error e_0 (26). The control design and computation are carried out as follows.

A Radial Basis Function (RBF) neural network with two inputs, x_1 and x_2, is used to directly estimate the ideal controller (14), which also corresponds to the adaptive control component defined in (15). Nine basis functions in the hidden layer are shown in Fig. 4.

A Radial Basis Function (RBF) neural network with two inputs, x_1 and x_2, is used to directly estimate the ideal controller (14), which also constitutes the adaptive control component (15). Nine basis functions in the hidden layer are shown in Fig. 4

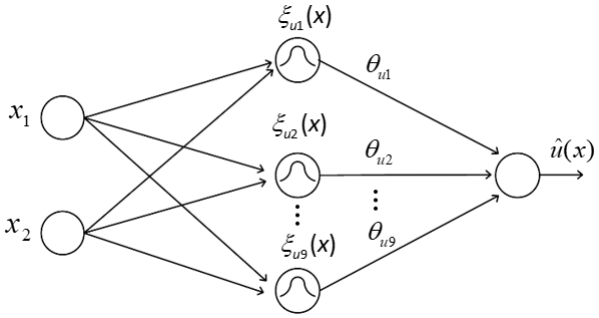

Fig. 4. The RBF neural network approximating the linearized feedback controller

In Fig. 4, the RBF network directly approximates the adaptive control law $\hat{u}$, and the output weights θ_u are updated online.

$$\hat{u} = \xi_u^T \theta_u \quad (15)$$

$\xi_u$represents the hidden layer's output.

$$\xi_u(x) = [\xi_{u1}(x)\ \xi_{u2}(x) \ldots \xi_{u9}(x)]^T \quad (16)$$

The following is the definition of the *i*-th RBF basis function.

$$\xi_{ui}(x) = e^{-\frac{[(x_1-\mu_{1i})^2+(x_2-\mu_{2i})^2]}{\sigma_i^2}} \quad (17)$$

These functions are chosen so that they distribute uniformly throughout the state space and the dispersions σ_i (i = 1…9) are chosen to be equal, choose $\sigma_i = \sigma$. The positions of the RBF neuron centers are distributed, as shown in Fig. 5.

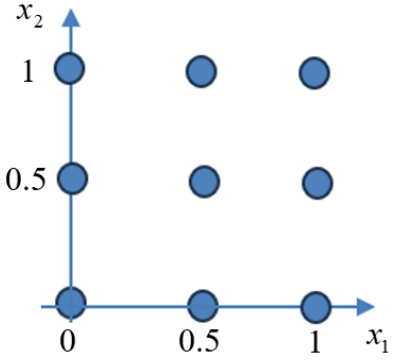

Fig. 5. The centers positions of the RBF neural network

θ_u is the weight vector of the output layer of the RBF network.

$$\theta_u = [\theta_{u1}\ \theta_{u2}\ \ldots\ \theta_{u9}]^T \quad (18)$$

The RBF network updates the vector θ_u online to get $\hat{u}$ closer to the optimal value u^*. There is a structural error in the network $\delta_u(x)$, because it is used to approximate the optimal control rule with limited RBF nodes,

$$u^*(x) = \theta_u^* \xi_u(x) + \delta_u(x) \quad (19)$$

Consequently, the following represents the variation between the achieved rule $\hat{u}$ along with the optimal rule u^*

$$\hat{u}(x) - u^*(x) = \tilde{\theta}_u \xi_u(x) - \delta_u(x) \quad (20)$$

With $\tilde{\theta}_u$ denoting the approximation error

$$\tilde{\theta}_u = \theta_u - \theta_u^* \quad (21)$$

Hypothesis 1: There is a continuous function $\bar{\delta}_u(x)$ since the RBFNN approximates the controller in a way that allows the top bound of the structural error $\delta_u(x)$ to be known beforehand in a manner that $|\delta_u(x)| \le \bar{\delta}_u(x), \forall x$.

Owing to structural error $\delta_u(x)$, we select the following control law to guarantee the system's stability.

$$u = \hat{u} + u_{sd} \quad (22)$$

Wherein u_{sd} is the sliding controller responsible for stabilizing the system, chosen such that the derivative of the Lyapunov function is negative semi-definite. From equation (4), it gives,

$$\ddot{y} = a(x) + b(x)u^*(t) + b(x)[u(t) - u^*(t)] \quad (23)$$

$$\ddot{y} = v(t) + b(x)[u(t) - u^*(t)]$$

Wherein $v(t) \in R$ denotes the dynamic system's input matrix, which has the following definition.

$$v(t) = \ddot{y}_d + \bar{e}_s + \eta e_s \quad (24)$$

With $\eta > 0, e_s$ and $\bar{e}_s$ are given by the following definitions.

$$e_s(t) = \dot{e}_0(t) + k_1 e_0(t) \quad (25)$$

$$e_0(t) = y_d(t) - y(t) \quad (26)$$

$$\bar{e}_s = \dot{e}_s - \ddot{e}_0 = k_1 \dot{e}_0 \quad (27)$$

Wherein $e_0(t)$ indicates the plant's output error and $e_s(t)$ indicates the track's erroneous value. The parameter k_1 is selected to satisfy the Routh-Hurwitz criteria. Here Hurwitz polynomial is: $\Delta_s = \dot{s} + k_1 s$.

Equations above-mentioned (27), (23)-(24), when combined, yield

$$\ddot{e}_0(t) = \ddot{y}_d(t) - \ddot{y}(t) \quad (28)$$

$$\ddot{e}_0(t) = \ddot{y}_d(t) - v(t) - b(x)[u(t) - u^*(t)] \quad (29)$$

$$\ddot{e}_0(t) = -\bar{e}_s - \eta e_s - b(x)[\hat{u}(t) + u_{sd}(t) - u^*(t)] \quad (30)$$

Following the substitution of (20) and (27) into (30), the tracking error's dynamic properties are given as follows.

$$\dot{e}_s + \eta e_s = -b\tilde{\theta}_u \xi_u(x) + b\delta_u(x) - b u_{sd} \quad (31)$$

Choosing a quadratic Lyapunov candidate as follows,

$$V = \frac{1}{2b} e_s^2 + \frac{1}{2} \tilde{\theta}_u^T Q_u \tilde{\theta}_u \quad (32)$$

With Q_u being a positive definite weighting matrix.

Hypothesis 2: $b(x)$ remains within a bounded range

$$0 < \underline{b}(x) \le b(x) \le \bar{b}(x) < \infty$$

Making a differentiation of the function V with respect to time yields

$$\dot{V} = \frac{1}{b} e_s \dot{e}_s - \frac{\dot{b}}{2b^2} e_s^2 + \tilde{\theta}_u^T Q_u \dot{\theta}_u \quad (33)$$

When (31) is inserted to $\dot{V}$, it gives,

$$\dot{V} = -\frac{\eta e_s^2}{b} - e_s u_{sd} + e_s \delta_u + \tilde{\theta}_u^T (Q_u \dot{\theta}_u - \xi_u e_s) - \frac{\dot{b}}{2b^2} e_s^2 \quad (34)$$

The following is the selection of the adaptive law.

$$\dot{\theta}_u = Q_u^{-1} \xi_u e_s \quad (35)$$

By inserting (35) into (34), we derive.

$$\dot{V} = -\frac{\eta e_s^2}{b} - e_s u_{sd} + e_s \delta_u - \frac{\dot{b}}{2b^2} e_s^2$$
$$\dot{V} \le -\frac{\eta e_s^2}{b} - e_s u_{sd} + |e_s|(|\delta_u| + \frac{|\dot{b}|}{2b^2}|e_s|)$$
$$\dot{V} \le -\frac{\eta e_s^2}{\bar{b}} - e_s u_{sd} + |e_s|(|\bar{\delta}_u| + \frac{\gamma_b}{2\underline{b}^2}|e_s|) \quad (36)$$

Hypothesis 3: There is a continuous function $\gamma_b(x)$ for which $|\dot{b}|(x) \le \gamma_b(x)$, and $b(x)$ has a limited fluctuation rate

Definition of the sliding mode controller

$$u_{sd} = (\bar{\delta}_u + \frac{\gamma_b}{2\underline{b}^2}|e_s|)\, sgn(e_s) \quad (37)$$

By inserting (37) into (36), we derive.

$$\dot{V} \le -\frac{\eta e_s^2}{\bar{b}} \le 0 \quad (38)$$

The system stays stable because *V* denotes a non-negative definite equation along with $\dot{V} \le 0$. Therefore, the Lyapunov stability theorem guarantees the ANSMC controller's stability.

Problem 2 formulation:

Trial and error is used to find σ_i, k_1, η and Q_u in equations (17), (25), (31), and (35) due to the controller's settings. As a result, it isn't easy to optimize these values. As explained in parts B and C, this study suggests using optimization methods to optimize these parameters to address this issue.

B. Evaluation of Optimization Techniques for EANSMC Controller Parameter Tuning Within the Coupled-Tank System

Five optimization techniques- PSO [59], GA [63], RAO 3 [68], FISA [71], and MDE [78] will be applied to optimally identify the ANSMC's parameters. All these methods have unique requirements and objective equations. To guarantee a fair comparison, each method is executed ten times from the same initial location. The average outcomes from these ten runs are then used to compare the method's convergence values.

Table II presents the parameters used in the simulations for the five optimization techniques: PSO, GA, RAO-3, FISA, and MDE, including both common and algorithm-specific parameters. An improper selection of these parameters may negatively impact the convergence quality of the algorithms. After testing, the parameters listed in this table provide the best convergence of the objective function for the considered optimization algorithms when tuning the controller parameters for the CTS system (1), under the physical constraints of the system, including the control input voltage $u \in [0, 24]$ V, and state variables $x_1,\ x_2 \in [0, 30]$ cm.

The following objective equation, used for all five algorithms, is chosen based on the ISE criterion evaluated over a 350-second duration. Objective function.

$$f = \int_0^t e_0^2(t)dt \quad (39)$$

with $e_0 = (y_d - y)$ from (26).

TABLE II. PARAMETERS USED FOR FIVE OPTIMIZATION TECHNIQUES

Method	Parameters	Value
General	Population size, NP	50
	Number of generations,	400
	Upper bound of 4 variables, $[k_1, \eta, \sigma, Q_u]$	[50, 20, 20, 100]
	Lower bound of 4 variables	[0.01, 0.01, 0.01, 1]
	Initial objective function value	13.552
PSO	Velocity update constant c_1, c_2	2
	Inertia weight	0.4
GA	Mutation rate	10%
	Crossover rate	90%
	Stall generation	200
	Convergence function tolerance	10^{-3}
RAO 3	No specific method parameters	
FISA	No specific method parameters	
MDE	Mutation coefficient, F	[0.4, 1]
	Crossover rate, CR	[0.7, 1]

Fig. 6 illustrates the comparative outcomes of ANSMC coefficients tuning, revealing that the FISA method produced the poorest convergent curve, while the MDE method exhibited the best and smallest convergence. Consequently, this study suggests the MDE optimization method to fine-tune the ANSMC's parameters, as elaborated in the subsequent subsection. The performance of the MDE algorithm can be significantly affected if the parameters CR and F in Table II are not appropriately selected. In this paper, the MDE algorithm [78] is employed, where the parameters CR and F are dynamically adjusted at random within the ranges [0.4, 1] and [0.7, 1], respectively, to enhance the algorithm's ability to search in many different directions. Additionally, the mutation phase of the standard DE algorithm is modified by combining two mutation strategies, rand/1 and best/1, to generate trial vectors, instead of using only a single mutation operator (either rand/1 or best/1) as in the standard DE. This modification aims to balance the global exploration and local exploitation capacities, thereby improving the ability to find the global optimum solution.

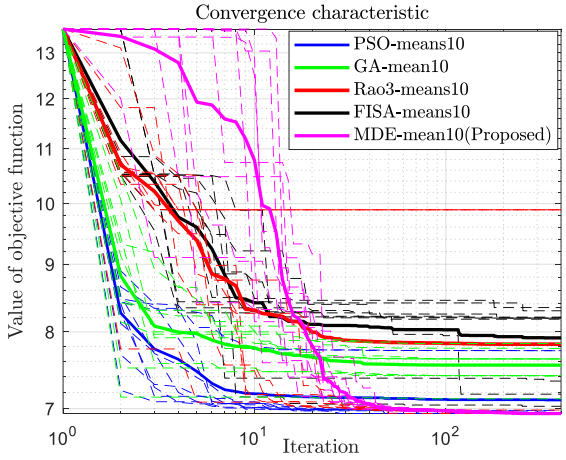

Fig. 6. Comparative results of various optimal approaches for ANSMC

C. DE Meta-Heuristic Method

The DE optimization method [72] effectively searches for the global optimum of objective functions, including non-differentiable ones. The following is a summary of the method.

1) Initialization: An Initial Population of NP Candidates, Each Expressed as a D-Dimensional Vector, is Generated at Random to Begin the DE Method

$$\vec{X}_{i,G} = (x_{1,i,G}, x_{2,i,G}, \ldots, x_{D,i,G}) \quad (40)$$

Every candidate $\vec{X}_{i,G}$represents an optimal solution with D variables limited within the bounds $x_{Min}$and x_{Max} . G is the number of evolution generations, where G = 0,1,2…,G_{Max}, I = 1,2,…,NP.

2) Mutation

The modified vector (the goal vector) for the i-th candidate is created by the randomized merging of three different vectors $\vec{X}_{r_1^i}$, $\vec{X}_{r_2^i}$,$\vec{X}_{r_3^i}$ from the present iteration population.

$$\vec{V}_{i,G} = \vec{X}_{r_1^i,G} + F(\vec{X}_{r_2^i,G} - \vec{X}_{r_3^i,G}) \quad (41)$$

The randomized integers r_1^i , r_2^i and r_3^i are random numbers within [1, NP]. Between either of the three vectors, the modified factor $F \in [0,1]$ lessens the difference.

3) Crossover

The crossover operation is carried out to enhance the variety within the population after the modified vector has been created. A test vector $\vec{U}_{i,G} = [u_{1,i,G}, u_{2,i,G}, \ldots, u_{3,i,G}]$ is produced by crossing the mutation-resulting vector $\vec{V}_{i,G}$ with a vector $\vec{X}_{i,G}$. The testing vector is usually created using the DE method using a binomial crossover strategy, which is explained as follows:

$$u_{j,i,G} = \begin{cases} v_{j,i,G} \text{ if } (\text{rand}_{j,i}[0,1] \le CR) \\ x_{j,i,G} \text{ otherwise} \end{cases} \quad (42)$$

Here, i=1, 2, …, NP; j= 1,2, …, D; CR stands for the Crossing Ratio, and $\text{rand}_{j,i}[0,1]$ is an arbitrary number.

4) Selection

A comparison is made between the target vector $\vec{X}_{i,G}$ and trial vector $\vec{U}_{i,G}$. The procedure for selection is described below.

$$\vec{X}_{i,G+1} = \begin{cases} \vec{U}_{i,G} \text{ if } f(\vec{U}_{i,G}) \le f(\vec{X}_{i,G}) \\ \vec{X}_{i,G} \end{cases} \quad (43)$$

Here, $f(\vec{X})$ denotes objective function.

5) Convergence

The entire process, including mutation, crossover, and selection, is carried out in a single iteration. The iterative cycle keeps going until one of the events listed below happens: the objective function reaches the desired minimal value, the quantity of generations approaches an upper limit, or the objective function stays constant for a meaningful amount of time.

D. ANSMC Controller Parameter Optimization with the Suggested Modified MDE Technique

In part C, the fundamental DE optimizing method [72] makes use of a predetermined crossover rate $CR = 0.7$and mutation coefficient $F = 0.4$. These two parameters, along with the population size NP, significantly impact the quality of the DE method.

The mutation coefficient F adjusts the amplitude of the differential vector when creating the mutated vector. A large F encourages exploration of a larger seeking area but may cause an early convergent curve. Conversely, a reduced F confines the search to a local area but increases convergent time. The crossover rate, CR, confirms the diverse particles. A high CR increases the likelihood of introducing new individuals into the population, expanding the search space, but possibly slowing convergence. On the other hand, a very low CR results in fewer new individuals entering the population, which could lead to premature convergence. Therefore, CR should be sufficiently large to ensure adequate search space while being small enough to allow for acceptable convergence time. This study suggests an MDE method [78] where F and CR are not fixed, as in the basic DE method [72], but change randomly after every generation with $F \in [0.4,1]$ and $CR \in [0.7,1]$ to enhance the optimization performance of the DE method.

Fig. 7 shows the structure of the ANSMC controller with parameters optimized using the MDE algorithm. The ANSMC controller parameters are optimized offline via the objective function (39). The flowchart of the proposed EANSMC-MDE algorithm is presented in Fig. 8.

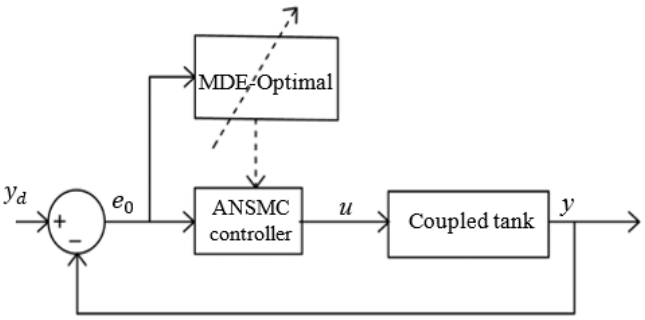

Fig. 7. The ANSMC Controller that has been optimized using the MDE method.

Fig. 8 illustrates the flowchart of the proposed EANSMC-MDE controller. First, the system state $x(t)$ is updated. Then, the output error e_0 in (26) and the sliding surface e_s in (25) are calculated. Next, this sliding surface is used to compute the adaptive law (35) to eliminate the approximation error $\tilde{\theta}_u$ in (21). Simultaneously, it is also employed to calculate the sliding control law u_{sd} in (37). Based on the adaptive law (35), the output weights θ_u of the RBFNN are updated. Afterward, the adaptive controller $\hat{u}$ in (15) is calculated. Subsequently, the overall ANSMC control law u in (22) is computed before being applied to control the CTS system. Finally, the control performance of the proposed algorithm is evaluated.

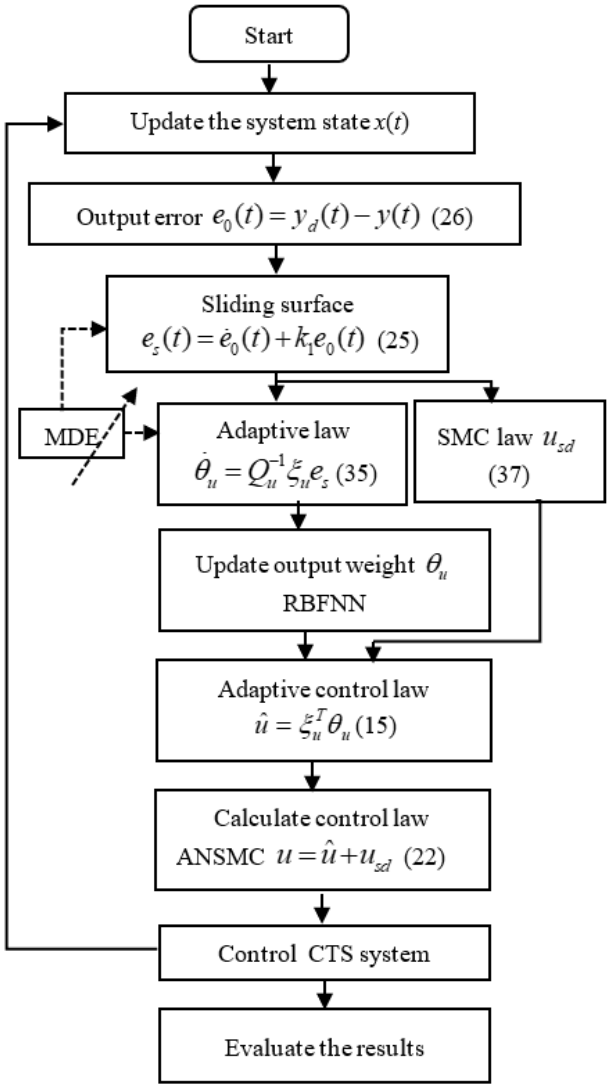

Fig. 8. The proposed EANSMC-MDE Controller flowchart

Fig. 9 presents the graph of the objective function after ten optimization runs of the ANSMC controller parameters over 400 generations, showing a consistent decrease in the objective function. Moreover, after around 200 generations, all runs exhibit the objective function values approaching the optimal and becoming nearly identical. Finally, convergence to the same objective value of 6.94026. This demonstrates the convergence capability of the proposed MDE method in tuning the parameters of the ANSMC controller. Among the runs, the 7th run, represented by the MDE6 curve, achieved the lowest convergence value of 6.9402062421618. The MDE method is designed to find the objective function's lowest value, and when the objective function (39) reaches its minimum, the error *e* also reaches its minimum. The results of the decision variables are as follows.

Table III presents the parameters of the ANSMC controller after being optimally tuned using the MDE algorithm. These parameters will be used in the simulations presented in Section IV. However, these parameters are no longer optimal when applied in real-time due to the variation of uncertain nonlinear factors during operation. In such cases, the ANSMC algorithm will adjust itself to adapt to these changes.

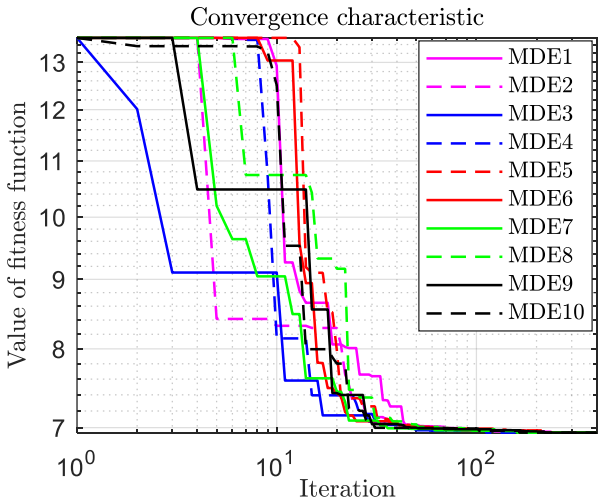

Fig. 9. Objective function while employing the MDE method to optimize the ANSMC controller's parameters

TABLE III. THE PARAMETERS OF THE ANSMC CONTROLLER AFTER BEING OPTIMALLY TUNED USING THE MDE ALGORITHM

Solution X	Decision variables			
	k_1	η	σ	Q_u
Value	0.01	6.5712	17.1839	21.1282

IV. SIMULATION RESULTS

The simulation of the EANSMC-MDE control system is carried out using the parameters of the ANSMC control system optimized by the MDE method in part D to control the CTS system. The results are compared with the ANSMC method and the SMC-MDE method, which is the conventional SMC technique (13) optimized by the MDE algorithm. Both controllers were parameter optimized using the same MDE settings as applied to the ANSMC control system.

Use a reference signal that was previously trained and varied over several levels to compare the CTS system's output response across several control methods.

Fig. 10 presents a comparison of the methods' output responses using the learned benchmark signal. Every method exhibits output tracking of the fluctuating benchmark test, which represents oscillating around the benchmark signal because of chattering. The EANSMC-MDE method achieves the fastest response, reaching steady-state within approximately 20 seconds, with zero steady-state error and no overshoot. Furthermore, the indexes of control quality for each method, as shown in Table IV, indicate that the EANSMC-MDE method outperforms the others in control quality. The methods will be further validated with an untrained reference signal, model parameter variations, and output sensor noise in the following sections.

TABLE IV. EVALUATION OF CONTROL QUALITY INDEXES ACROSS DIFFERENT METHODS

Quality Indexes	EANSMC-MDE	ANSMC	SMC-MDE
IAE	**249.4**	263	320.5
ISE	**1300**	1358	1676
ITAE	**$3.958*10^4$**	$4.313*10^4$	$5.42*10^4$

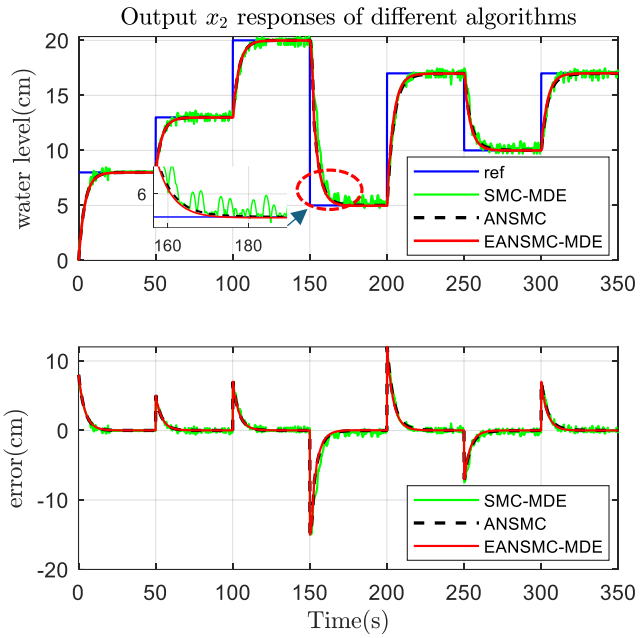

Fig. 10. Evaluation of the CTS system's output performance across different methods using the trained benchmark

- Validate the output response results with varying and untrained reference signals.
- Validate the output response results with an untrained reference signal, output sensor noise, and varying model disturbing the outlet valve area b_2 of Tank 2 in Fig. 12, Fig. 13 to Fig. 14.

Fig. 11 presents a comparison of output response curves among the methods with the not-yet-trained reference signal. Despite more significant variations in the reference signal than the trained signal, the output response of EANSMC-MDE remains fast, without overshooting, and with zero steady-state error. Meanwhile, between 100 and 150 seconds, the SMC-MDE method exhibits an undershoot response.

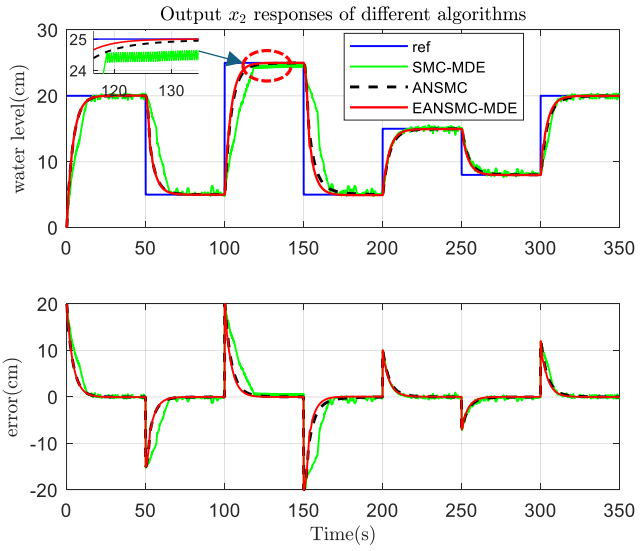

Fig. 11. The CTS system output x_2 response to an untrained reference signal

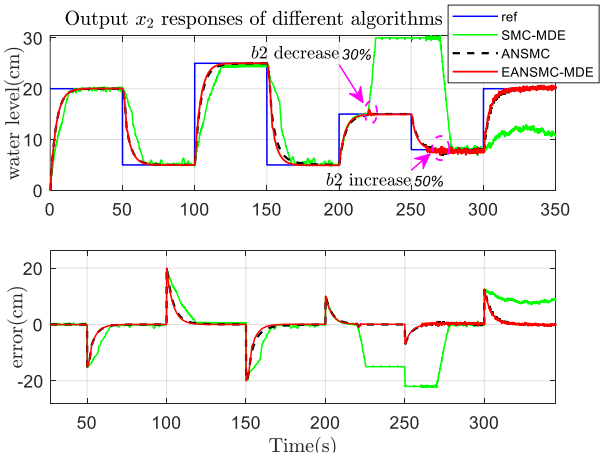

Fig. 12. The CTS system output x_2 response to output sensor noise and disturbance drain b_2 with an untrained reference signal

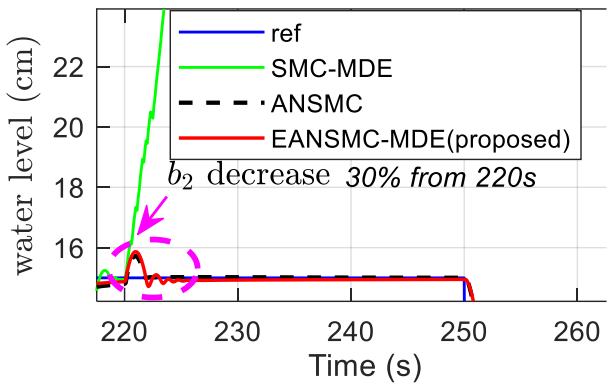

Fig. 13. CTS system output x_2 response to output sensor noise and decrease drain b_2 with untrained reference signal (zooming from Fig. 12)

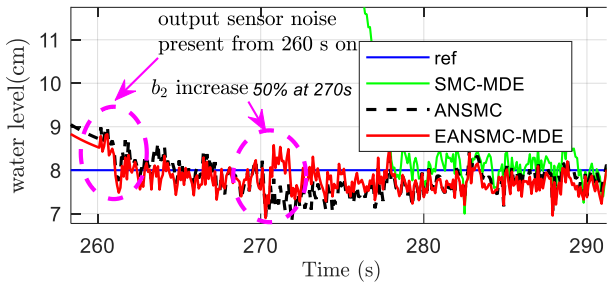

Fig. 14. CTS system output x_2 response to output sensor noise and increase drain b_2 with untrained reference signal (zooming from Fig. 12)

Fig. 13 and Fig. 14 are zoomed pictures from Fig. 12, depicting the valve opening of Tank 2 decreasing 30% from 220 seconds and increasing 50% from 270 seconds. Consequently, the output response of the EANSMC-MDE and ANSMC overshoot lasted for about 1.5 seconds before returning to a steady state. Meanwhile, the SMC-MDE method becomes unstable from 220 seconds onwards. This is because the traditional SMC algorithm (13) depends on the mathematical model of the controlled system. Therefore, when the model parameters change significantly along with variations in the reference signal, the system becomes unstable. In such cases, the controller parameters need to be re-tuned appropriately so that the system may respond properly, depending on the specific conditions. With the presence of output sensor noise starting at 260 seconds, with

a zero mean and variance of 0.05, the output responses of the EANSMC-MDE and ANSMC methods oscillate around the reference signal. Additionally, when the drain increases by 50% from 270 seconds onwards, the outputs oscillate more for about 3 seconds, then stabilize around the reference signal under the influence of output sensor noise.

Fig. 15 presents the responses of the nine output weights θ_u of the RBF network in the EANSMC-MDE controller under the influence of output sensor noise and disturbance drain b_2 of Tank 2 with an untrained signal. These results indicate that when there are changes in the reference signal, output sensor noise, or model parameters, these weights respond quickly to help the system return to a stable state and track the reference signal.

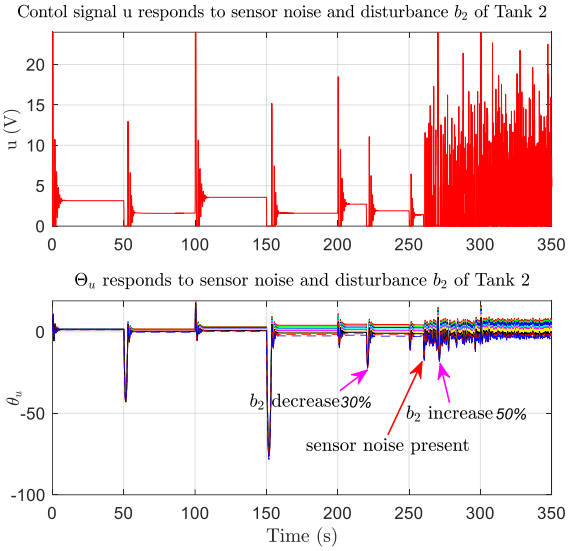

Fig. 15. CTS system output x_2 response to output sensor noise and disturbance drain b_2 of Tank 2 with an untrained reference signal

- Validate the output response results with an untrained reference signal, output sensor noise change to simulate measurement noise that may be present in a real system, and Gaussian noise with zero mean and a variance of 0.1 is added [80]. In addition, further validation is conducted for cases where the noise level increases by a factor of 2 to 8, corresponding to variances of 0.2, 0.4, and 0.8.
- Validate the output response results with an untrained reference signal and varying model disturbing the outlet valve area b_2 of Tank 2

The following simulation results validate the output response of x_2 to a high-level reference signal under the influence of the gradual increase of the outlet valve area b_2 of Tank 2.

Fig. 16 presents the validation results of the output response when the output sensor signal is corrupted by noise with increasing variance from 0.1 to 0.8. Table V summarizes the total error using the ISE criterion corresponding to each variance level. When the variance is 0.1, the output tracks the reference signal well, with a total error of 3958. If the variance is doubled, the error increases by 10%. However, as the variance continues to rise, the error grows rapidly. When the variance reaches 0.8, the error increases by 44% compared to the case with a variance of 0.1. The zoomed view in Fig. 16 shows that as the variance increases, the output's ability to track the reference signal, particularly during significant transitions from 5 cm to 25 cm, significantly deteriorates. This indicates that the higher the amplitude of sensor noise, the more it negatively affects the output tracking performance of the system.

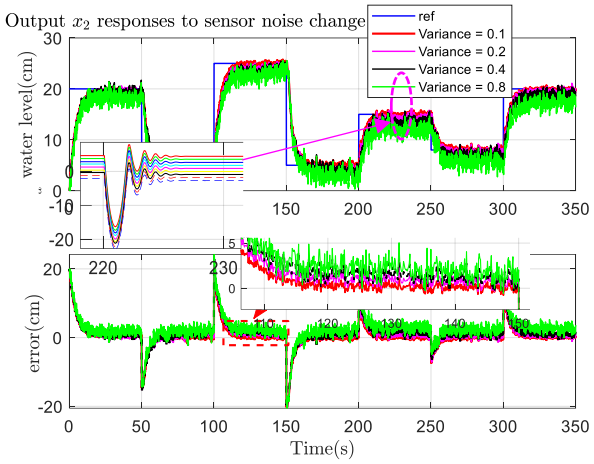

Fig. 16. CTS system output x_2 response to output sensor noise change variance with an untrained reference signal

TABLE V. EVALUATION OF CONTROL QUALITY INDEXES ACROSS OUTPUT SENSOR NOISE CHANGE VARIANCE

Variance	0.1	0.2	0.4	0.8
ISE	3958	4346	5035	6765
Increase		10%	17%	44%

Fig. 17 shows that when the outlet valve area b_2 of Tank 2 increases from 0.7 cm² to 1.2 cm², the water level x_1 in Tank 1 rises to approximately 28.7 cm. At this point, the output x_2 closely tracks the reference signal Ref = 20 cm. When b_2 increases from 0.7 cm² to 1.2247 cm², x_1 further increases to x_{1max} cm, while the output x_2 still maintains good tracking of the reference Ref = 20 cm. However, when b_2 increases from 0.7 cm² to 1.25 cm², x_1 reaches its maximum level x_{1max} cm, but x_2 can no longer track the reference signal Ref = 20 cm and only maintains at 19.2 cm.

These results can be explained by the physical constraints of the CTS system (1) as follows:

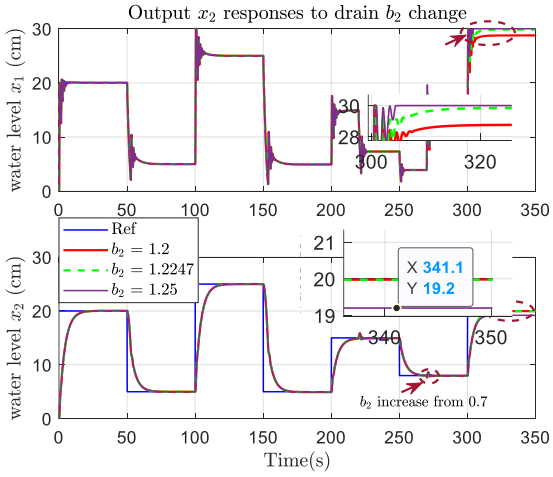

Fig. 17. CTS system output x_2 response to increased drain b_2 with an untrained reference signal

The controller is responsible for ensuring that the output x_2 tracks the reference, Ref. When the output x_2 reaches a specific value $x_2 = x_{20}$, x_{20} may or may not coincide with Ref, depending on the controller's capability and the physical limitations of the CTS system. At that time, the differential equation $\dot{x}_2 = \frac{1}{A_2}(b_1C_1\sqrt{2gx_1} - b_2C_2\sqrt{2gx_2})$ of the CTS system (1) becomes

$$\frac{1}{A_2}(b_1C_1\sqrt{2gx_1} - b_2C_2\sqrt{2gx_{20}}) = 0 \quad (44)$$

From (44), x_{20} is obtained as follows:

$$x_{20} = \left(\frac{b_1C_1}{b_2C_2}\right)^2 x_1 \quad (45)$$

When the outlet valve area b_2 increases, the controller attempts to increase x_1 accordingly so that x_{20} reaches the reference value, Ref. However, x_1 is limited by its physical constraint $x_1 = x_{1max}$. If b_2 continues to increase beyond the limit b_{2max} as defined in (46), then x_{20} still cannot reach the reference value, Ref, even though the controller has already driven x_1 to its maximum $x_1 = x_{1max}$.

$$Ref = x_{20} = \left(\frac{b_1C_1}{b2_{2max}}()^2{}_{1max}\right) \quad (46)$$

Alternatively, to ensure x_{20} = Ref, the maximum value b_{2max} is determined as follows.

$$b\frac{b_1C_1}{C_2}\sqrt{\frac{x_{1max}}{Ref}}_{2max} \quad (47)$$

When $x_1 = x_{1max}$ cm, to achieve x_{20} = Ref = 20 cm, from (47), we obtain b_{2max} cm². When increasing b_2 beyond this value, for example, b_2= 1.25 cm², with $x_1 = x_{1max}$ cm, $b_1 = 1$ cm² and $C_1 = C_2 = 0.8$ cm² (from Table I). From (45), x_2 can be calculated as 19.2 cm. In this case, x_2 cannot reach the reference value Ref = 20 cm. Therefore, in order for x_2 to reach Ref = 20 cm, b_2 must not exceed this limit of b_{2max} cm². These calculations confirm the simulation results shown in Fig. 17. Hence, when changing Ref or modifying parameters of the CTS system model (1), in order to track Ref, the physical constraint (45) must be satisfied. When only Ref and b_2 are varied, these two quantities must satisfy condition (48)

$$\left\{Ref = x_{20} \le \left(\frac{b_1C_1}{b2_{2max}}()^2{}_{1max}\middle| b_2 \le b\frac{b_1C_1}{C_2}\sqrt{\frac{x_{1max}}{Ref}}_{2max}\right\}\right) \quad (48)$$

The above simulation results clearly demonstrate that the EANSMC-MDE method surpasses the other methods in terms of output response characteristics and performs well with both changing reference signals and untrained signals, as shown in Fig. 10 and Fig. 11. Next, the online adaptive capability of the EANSMC-MDE method is validated by varying the model parameters and output sensor noise in Fig. 12, Fig. 13, Fig. 14 to Fig. 15 demonstrates the rapid and effective response capabilities of the RBF network to various disturbances, demonstrating the controller's effective online adaptation. Moreover, Fig. 16 presents the system's output response when sensor noise increases several times compared to the levels that could be present in the real system model [80], resulting in a rapid rise in output tracking error, which leads to a significant reduction in control performance. Furthermore, Fig. 17 shows the output response when the reference signal undergoes large changes and the outlet valve parameter varies significantly beyond the physical limits of the system, causing the output to fail to follow the reference. To ensure control performance, these variations must satisfy the physical constraint conditions (45) and (48) of the CTS system (1). The above simulation results demonstrate that the proposed controller can provide satisfactory performance under output sensor noise, external disturbances that cause variations in model parameters, and changes in reference signals—conditions that may occur in a real-world uncertain nonlinear system, provided that these changes remain within the system's physical constraints. Furthermore, the proposed controller, as designed in Section III.A, does not require the mathematical model of the plant. Therefore, the proposed method holds promise for application to other uncertain nonlinear MISO/MIMO systems.

V. CONCLUSION

The EANSMC-MDE method for liquid level control in a CTS system, which is a nonlinear system with high delays and several uncertainties, such as load variations, model parameter variations, sensor noise, etc., is suggested in this study. The proposed method integrates the ANSMC method optimized via the MDE optimization method. This optimization method is compared with other meta-heuristic methods such as PSO, GA, RAO-3, and FISA. The controller was designed using the Lyapunov stability theorem to guarantee system stability. Benchmark tests applied to the suggested method, the ANSMC and conventional SMC, all optimized with the MDE method under the same settings as the ANSMC method, were carried out to show the efficacy of the suggested method. According to simulation results, the suggested method produces a quick output response with no overshoot and no steady-state inaccuracy. Most control quality indices perform superior compared to the results of other methods. Moreover, the system output responds well despite significant changes in the reference signal, regardless of prior training. Additionally, the results verified with varying model parameters and output sensor noise demonstrate the good adaptive capability of the proposed controller. As a result, the suggested EANSMC-MDE method validates its capacity for efficient application in controlling a variety of additional nonlinear MISO and MIMO systems. However, if the sensor noise variance is increased to several times higher than the level that could exist in a real system [80], the response quality of the system significantly deteriorates. Additionally, when the reference signal undergoes large changes, if the system parameters are altered excessively beyond the physical limits of the system, the output cannot follow the reference even if the controller performs well. The strength of the proposed algorithm lies in its ability to provide stable control performance right from the initialization phase, thanks to the parameters having been optimized beforehand. However, the limitation is that the ANSMC controller parameters are optimally tuned offline

using the MDE algorithm. Therefore, a model of the system is required for parameter optimization. As a result, when applying the controller to a real system, the system model must first be identified before applying MDE to tune the controller parameters. Moreover, these optimized parameters may no longer remain optimal when the system encounters changing uncertainties during real-time operation. Nevertheless, the ANSMC controller is capable of compensating for such varying uncertainties through approximation, thereby maintaining control quality. Furthermore, the proposed MDE optimization algorithm [78] relies on the dynamic adjustment of parameters F and CR, but its performance has not been verified under different variations of these parameters. Future work will focus on applying the proposed algorithm to real systems, systems with fast dynamic responses, by incorporating nonsingular terminal sliding mode control to regulate the convergence time of the system.

ACKNOWLEDGMENT

We acknowledge Ho Chi Minh City University of Technology (HCMUT), VNU-HCM, for supporting this study.

REFERENCES

[1] K. R. A. Govind, S. Mahapatra, and S. R. Mahapatro, "Design of an Optimal Control Strategy for Coupled Tank Systems Using Nonlinear Constraint Optimization With Kharitonov-Hurwitz Stability Analysis," *IEEE Access*, vol. 11, pp. 72618-72629, 2023.

[2] K. R. A. Govind and S. J. S. Mahapatra, "Frequency domain specifications-based robust decentralized PI/PID control algorithm for benchmark variable-area coupled tank systems," *Sensors*, vol. 22, no. 23, p. 9165, 2022.

[3] J. Sánchez-Palma and J. L. Ordoñez-Ávila, "A PID Control Algorithm With Adaptive Tuning Using Continuous Artificial Hydrocarbon Networks for a Two-Tank System," *IEEE Access*, vol. 10, pp. 114694-114710, 2022.

[4] S. A. Al-Samarraie and I. I. Gorial, "Assessment of FLC, PID, Nonlinear PID, and SMC controllers for level stabilization in mechatronic systems," *Journal of Robotics and Control*, vol. 5, no. 6, pp. 1845-1861, 2024.

[5] T. R. D. Kumar and S. J. Mija, "Boundary Logic-Based Hybrid PID-SMC Scheme for a Class of Underactuated Nonlinear Systems-Design and Real-Time Testing," *IEEE Transactions on Industrial Electronics*, vol. 72, no. 5, pp. 5257-5267, 2025.

[6] T. R. D. Kumar and S. J. Mija, "Synthesis and experimental demonstration of a hybrid adaptive PID-SMC algorithm for a class of underactuated nonlinear systems," *Nonlinear Nonlinear Dynamics*, vol. 113, no. 12, pp. 15037–15056, 2025.

[7] K. D. Wahyuadnyana, K. Indriawati, P. A. Darwito, A. N. Aufa, and H. Tnunay, "Performance analysis of PID and SMC control algorithms on AUV under the influence of internal solitary wave in the Bali Deep Sea," *Journal of Robotics and Control*, vol. 5, no. 6, pp. 1957–1972, 2024.

[8] A. Ardjal, M. Bettayeb, R. Mansouri, and B. Zouak, "Design and implementation of a model-free fractional order intelligent PI fractional order sliding mode controller for water level tank system," *ISA Transactions*, vol. 127, pp. 501–510, 2022.

[9] B. Gurjar, V. Chaudhari, and S. Kurode, "Parameter estimation-based robust liquid level control of quadruple tank system—Second-order sliding mode approach," *Journal of Process Control*, vol. 104, pp. 1–10, 2021.

[10] S. Kamal, T. Haque, and L. Chen, "Discrete-time control with application to coupled tank system: A ceiling function approach," *SSRN*, 2023.

[11] V. K. Singh, S. Kamal, B. Bandyopadhyay, S. Ghosh, and T. N. Dinh, "Prescribed-Time Optimal Control of Nonlinear Dynamical Systems With Application to a Coupled Tank System," *IEEE Transactions on Automation Science and Engineering*, vol. 22, pp. 191-201, 2025.

[12] X. Meng, H. Yu, J. Zhang, T. Xu, and H. Wu, "Liquid level control of four-tank system based on active disturbance rejection technology," *Measurement*, vol. 175, p. 109146, 2021.

[13] X. Meng, H. Yu, J. Zhang, T. Xu, H. Wu, and K. Yan, "Disturbance observer-based feedback linearization control for a quadruple-tank liquid level system," *ISA Transactions*, vol. 122, pp. 146–162, 2022.

[14] X. Meng, H. Yu, T. Xu, and H. Wu, "Disturbance observer and L2-gain-based state error feedback linearization control for the quadruple-tank liquid-level system," *Energies*, vol. 13, no. 20, p. 5500, 2020.

[15] X. Meng, H. Yu, H. Wu, and T. Xu, "Disturbance observer-based integral backstepping control for a two-tank liquid level system subject to external disturbances," *Mathematical Problems in Engineering*, vol. 2020, no. 1, pp. 1-22, 2020.

[16] B. Tacal and L. Ucun, "Bernstein polynomials-based compensator design for coupled tank system with saturation nonlinearity," *Proceedings of the Institution of Mechanical Engineers, Part I*, vol. 236, no. 7, pp. 1274–1284, 2022.

[17] R. Raj, A. Kumar, D. Sharma, and S. Khan, "TS fuzzy controller with S- and Z-type MFs to control a coupled-tank system," *Materialstoday: Proceedings*, vol. 80, pp. A8–A13, 2023.

[18] D. S. Bhandare, N. R. Kulkarni, and M. V. Bakshi, "Hardware implementation of a novel intelligent fuzzy fractional order proportional-integral (FFOPI) controller for a coupled tank liquid level control system," *Sādhanā*, vol. 49, no. 4, p. 296, 2024.

[19] Q. N. Duong and N. T. Dang, "Model-free optimal control for underactuated quadrotor aircraft via reinforcement learning," *Journal of Robotics and Control*, vol. 5, no. 6, pp. 1827–1835, 2024.

[20] K. Phothongkum and S. Kuntanapreeda, "Stability-constrained reinforcement learning for level control of nonlinear coupled tank system: An experimental study," *Neural Computing and Applications*, vol. 37, no. 6, pp. 4277–4290, 2025.

[21] L. N. Tan, T. P. Cong, and D. P. Cong, "Neural Network Observers and Sensorless Robust Optimal Control for Partially Unknown PMSM With Disturbances and Saturating Voltages," *IEEE Transactions on Power Electronics*, vol. 36, no. 10, pp. 12045-12056, 2021.

[22] L. N. Tan and T. C. Pham, "Optimal Tracking Control for PMSM With Partially Unknown Dynamics, Saturation Voltages, Torque, and Voltage Disturbances," *IEEE Transactions on Industrial Electronics*, vol. 69, no. 4, pp. 3481-3491, 2022.

[23] L. N. Tan, N. Gupta, and M. Derawi, "H∞ Control for Oscillator Systems With Event-Triggering Signal Transmission of Internet of Things," *IEEE Access*, vol. 11, pp. 8938-8949, 2023.

[24] L. N. Tan, H. -T. Tran, and T. -T. Tran, "Event-Triggered Observers and Distributed H∞ Control of Physically Interconnected Nonholonomic Mechanical Agents in Harsh Conditions," *IEEE Transactions on Systems, Man, and Cybernetics: Systems*, vol. 52, no. 12, pp. 7871-7884, 2022.

[25] S. Zeghlache, M. Z. Ghellab, A. Djerioui, B. Bouderah, and M. F. Benkhoris, "Adaptive fuzzy fast terminal sliding mode control for inverted pendulum-cart system with actuator faults," *Mathematics and Computers in Simulation*, vol. 210, pp. 207–234, 2023.

[26] X. Su, X. Yang, and Y. Xu, "Fuzzy adaptive terminal sliding mode control based on recurrent neural network compensation for a maglev system," *Engineering Applications of Artificial Intelligence*, vol. 124, p. 106588, 2023.

[27] Z. Wu, B. Jiang, and Q. Gao, "State estimation and fuzzy sliding mode control of nonlinear Markovian jump systems via adaptive neural network," *Journal of the Franklin Institute*, vol. 359, no. 16, pp. 8974–8990, 2022.

[28] B. Jiang, H. R. Karimi, X. Zhang, and Z. Wu, "Adaptive neural-network-based sliding mode control of switching distributed delay systems with Markov jump parameters," *Neural Networks*, vol. 165, pp. 846-859, 2023.

[29] M. S. Mahmoud, M. Maaruf, and S. El-Ferik, "Neuro-adaptive output feedback control of the continuous polymerization reactor subjected to parametric uncertainties and external disturbances," *ISA Transactions*, vol. 112, pp. 1-11, 2021.

[30] S. Ullah, Q. Khan, A. Mehmood, S. A. M. Kirmani, O. Mechali, R. Ahmed, and K. Hussain, "Neuro-adaptive fast integral terminal sliding

mode control design with variable gain robust exact differentiator for under-actuated quadcopter UAV," *ISA Transactions*, vol. 120, pp. 293-304, 2022.

[31] B. Gao, Y.-J. Liu, and L. Liu, "Adaptive neural fault-tolerant control of a quadrotor UAV via fast terminal sliding mode," *Aerospace Science and Technology*, vol. 129, p. 107818, 2022.

[32] J. Hu, D. Zhang, Z. Wu, and H. Li, "Neural network-based adaptive second-order sliding mode control for uncertain manipulator systems with input saturation," *ISA Transactions*, vol. 136, pp. 126-138, 2023.

[33] J. Wang, T. P. Zhu, B. He, G. Deng, C. Zhang, and X. Huang, "An adaptive neural sliding mode control with ESO for uncertain nonlinear systems," *International Journal of Control, Automation and Systems*, vol. 19, pp. 687–697, 2021.

[34] D. T. Tran, H. N. Tong, and K. K. Ahn, "An extended state observer-based on the terminal sliding mode control for 6-DOF manipulator against lumped uncertainties," *International Journal of Control, Automation and Systems*, vol. 23, no. 3, pp. 810-823, 2025.

[35] S. Choueikh, M. Kermani, and F. M'sahli, "A comparative study of nonsingular terminal sliding mode and backstepping schemes for the coupled two-tank system," *Complexity*, vol. 2021, no. 1, pp. 1–18, 2021.

[36] M. Tao, X. He, S. Xie, and Q. Chen, "RBFNN-based singularity-free terminal sliding mode control for uncertain quadrotor UAVs," *Computational Intelligence and Neuroscience*, vol. 2021, no. 1, pp. 1-10, 2021.

[37] Z. Liu, X. Gong, and J. Fei, "Nonsingular fast terminal sliding mode control of DC–DC buck converter using fuzzy neural network and disturbance observer," *Nonlinear Dynamics*, vol. 113, no. 11, pp. 13389–13414, 2025.

[38] I. U. Haq *et al*., "Neural network-based adaptive global sliding mode MPPT controller design for stand-alone photovoltaic systems," *PloS ONE*, vol. 17, no. 1, p. e0260480, 2022.

[39] Z. Han, S. Li, and H. Liu, "Composite learning sliding mode synchronization of chaotic fractional-order neural networks," *Journal of Advanced Research*, vol. 25, pp. 87–96, 2020.

[40] B. Li, X. Zhao, and M. Wu, "Adaptive neural network sliding mode control for a class of SISO nonlinear systems," *Mathematics*, vol. 10, no. 7, p. 1182, 2022.

[41] M. Yang, X. Zhang, Y. Xia, Q. Liu, and Q. Zhu, "Adaptive neural network-based sliding mode control for a hydraulic rotary drive joint," *Computers and Electrical Engineering*, vol. 102, p. 108189, 2022.

[42] S. Chaudhuri, R. Saha, A. Chatterjee, S. Mookherjee, and D. Sanyal, "Adaptive neural-bias-sliding mode control of rugged electrohydraulic system motion by recurrent Hermite neural network," *Control Engineering Practice*, vol. 103, p. 104588, 2020.

[43] J. Fu, F. Huang, and Z. Chen, "Optimization-based adaptive neural sliding mode control for nonlinear systems with fast and accurate response under state and input constraints," *Journal of the Franklin Institute*, vol. 359, no. 13, pp. 6735–6758, 2022.

[44] A. Merabet, S. Kanukollu, A. Al-Durra, and E. F. El-Saadany, "Adaptive recurrent neural network for uncertainties estimation in feedback control system," *Journal of Automation and Intelligence*, vol. 2, no. 3, pp. 119–129, 2023.

[45] S. C. Yogi, V. K. Tripathi, and L. Behera, "Adaptive Integral Sliding Mode Control Using Fully Connected Recurrent Neural Network for Position and Attitude Control of Quadrotor," *IEEE Transactions on Neural Networks and Learning Systems*, vol. 32, no. 12, pp. 5595-5609, 2021.

[46] T. Kang, H. Peng, F. Zhou, X. Tian, and X. Peng, "Robust predictive control of coupled water tank plant," *Applied Intelligence*, vol. 51, pp. 5726–5744, 2021.

[47] P. Singh, D. K. Giri, and A. K. Ghosh, "Robust backstepping sliding mode aircraft attitude and altitude control based on adaptive neural network using symmetric BLF," *Aerospace Science and Technology*, vol. 126, p. 107653, 2022.

[48] A. Baraean *et al*., "Physics-informed NN-based adaptive backstepping terminal sliding mode control of buck converter for PEM electrolyzer," *Heliyon*, vol. 10, no. 7, p. e29254, 2024.

[49] W. Ruan, Q. Dong, X. Zhang, and Z. Li, "Friction compensation control of electromechanical actuator based on neural network adaptive sliding mode," *Sensors*, vol. 21, no. 4, p. 1508, 2021.

[50] Z. Zhu, Z. Duan, H. Qin, and Y. Xue, "Adaptive neural network fixed-time sliding mode control for trajectory tracking of underwater vehicle," *Ocean Engineering*, vol. 287, p. 115864, 2023.

[51] V. B. V. Nghia, T. V. Thien, N. N. Son, and M. T. Long, "Adaptive neural sliding mode control for two-wheel self-balancing robot," *International Journal of Dynamics and Control*, vol. 10, no. 3, pp. 771–784, 2022.

[52] Z. Zhao and X. Jin, "Adaptive neural network-based sliding mode tracking control for agricultural quadrotor with variable payload," *Computers and Electrical Engineering*, vol. 103, p. 108336, 2022.

[53] S. Liu, L. Zhang, B. Niu, X. Zhao, and A. M. Ahmad, "Adaptive neural finite-time hierarchical sliding mode control of uncertain under-actuated switched nonlinear systems with backlash-like hysteresis," *Information Sciences*, vol. 599, pp. 147–169, 2022.

[54] L. Shanmugam and Y. H. Joo, "Adaptive neural networks-based integral sliding mode control for TS fuzzy model of delayed nonlinear systems," *Applied Mathematics and Computation*, vol. 450, p. 127983, 2023.

[55] A. Zheng, Y. Huang, J. Na, and Q. Shi, "Adaptive neural identification and non-singular control of pure-feedback nonlinear systems," *ISA Transactions*, vol. 144, pp. 409-418, 2024.

[56] H. Feng *et al*., "A new adaptive sliding mode controller based on the RBF neural network for an electro-hydraulic servo system," *ISA Transactions*, vol. 129, pp. 472–484, 2022.

[57] N. V. Quan and N. N. Son, "Control of a DC–DC buck converter using adaptive neural network," *Electrical Engineering*, 2024.

[58] K. A. Sundari and P. Maruthupandi, "Optimal design of PID controller for the analysis of two-tank system using metaheuristic optimization algorithm," *Journal of Electrical Engineering & Technology*, vol. 17, no. 1, pp. 627–640, 2022.

[59] S. L. Narayanan, M. Kasiselvanathan, K. B. Gurumoorthy, and V. Kiruthika, "Particle swarm optimization based artificial neural network (PSO-ANN) model for effective k-barrier count intrusion detection system in WSN," *Measurement: Sensors*, vol. 29, p. 100875, 2023.

[60] T. Zong, J. Li, and G. Lu, "Auxiliary model-based multi-innovation PSO identification for Wiener–Hammerstein systems with scarce measurements," *Engineering Applications of Artificial Intelligence*, vol. 106, p. 104470, 2021.

[61] R. Cortez, R. Garrido, and E. Mezura-Montes, "Spectral richness PSO algorithm for parameter identification of dynamical systems under non-ideal excitation conditions," *Applied Soft Computing*, vol. 128, p. 109490, 2022.

[62] T. Zong, J. Li, and G. Lu, "Parameter estimation of multivariable Wiener nonlinear systems by the improved particle swarm optimization and coupling identification," *Information Sciences*, vol. 661, p. 120192, 2024.

[63] A. Tanveer and S. M. Ahmad, "High fidelity modeling and GA optimized control of yaw dynamics of a custom-built remotely operated unmanned underwater vehicle," *Ocean Engineering*, vol. 266, p. 112836, 2022.

[64] X.-Q. Zhang, Q. Cheng, W. Sun, Y. Zhao, and Z. Li, "Research on a TOPSIS energy efficiency evaluation system for crude oil gathering and transportation systems based on a GA-BP neural network," *Petroleum Science*, vol. 21, no. 1, pp. 621–640, 2024.

[65] Z. Ma, X. Li, and J. Sun, "A data-driven fault detection approach for unknown large-scale systems based on GA-SVM," *Information Sciences*, vol. 658, p. 120023, 2024.

[66] S. Chauhan, B. Singh, and M. Singh, "Modified ant colony optimization-based PID controller design for coupled tank system," *Engineering Research Express*, vol. 3, no. 4, p. 045005, 2021.

[67] A. G. K. R and S. Mahapatra, "Improving precision and robustness in level control of coupled tank systems: A tree seed optimization and μ-analysis approach," *Results in Control and Optimization*, vol. 15, p. 100410, 2024.

[68] R. V. Rao, "Rao algorithms: Three metaphor-less simple algorithms for solving optimization problems," *International Journal of Industrial Engineering Computations*, vol. 11, no. 1, pp. 107–130, 2020.

[69] S. Sahay, R. Upputuri, and N. Kumar, "Optimal power flow-based approach for grid dispatch problems through Rao algorithms," *Journal of Engineering Research*, vol. 11, no. 2, p. 100032, 2023.

[70] A. Farah, A. Belazi, F. Benabdallah, A. Almalaq, M. Chtourou, and M. A. Abido, "Parameter extraction of photovoltaic models using a comprehensive learning Rao-1 algorithm," *Energy Conversion and Management*, vol. 252, p. 115057, 2022.

[71] M. Ghasemi *et al*., "A new metaphor-less simple algorithm based on Rao algorithms: A fully informed search algorithm (FISA)," *PeerJ Computer Science*, vol. 9, p. e1431, 2023.

[72] C. Van Kien, H. P. H. Anh, and N. N. Son, "Adaptive inverse multilayer fuzzy control for uncertain nonlinear system optimizing with differential evolution algorithm," *Applied Intelligence*, vol. 51, no. 1, pp. 527–548, 2021.

[73] C. D. Iweh and E. R. Akupan, "Control and optimization of a hybrid solar PV–hydro power system for off-grid applications using particle swarm optimization (PSO) and differential evolution (DE)," *Energy Reports*, vol. 10, pp. 4253–4270, 2023.

[74] W. Deng, J. Xu, Y. Song, and H. Zhao, "Differential evolution algorithm with wavelet basis function and optimal mutation strategy for complex optimization problem," *Applied Soft Computing*, vol. 100, p. 106724, 2021.

[75] H. Zhang, Z. Gao, Y. Pan, G. Yang, W. J. (Chris) Zhang, and J. Wang, "A synergy of the adaptive whale optimization algorithm and differential evolution for abrupt motion tracking," *Applied Soft Computing*, vol. 144, p. 110554, 2023.

[76] S. Gao, K. Wang, S. Tao, T. Jin, H. Dai, and J. Cheng, "A state-of-the-art differential evolution algorithm for parameter estimation of solar photovoltaic models," *Energy Conversion and Management*, vol. 230, p. 113784, 2021.

[77] N. Li, H. Yang, W. Zhu, and C. Liu, "A novel grey decision-DE optimized internal model controller for vibration control of nonlinear uncertain aeroelastic blade system," *ISA Transactions*, vol. 107, pp. 27–39, 2020.

[78] N. N. Son, "Level control of quadruple tank system based on adaptive inverse evolutionary neural controller," *International Journal of Control, Automation and Systems*, vol. 18, no. 9, pp. 2386–2397, 2020.

[79] N. N. Son, H. P. H. Anh, and C. V. Kien, "Adaptive sliding mode control with hysteresis compensation-based neuro-evolution for motion tracking of piezoelectric actuator," *Applied Soft Computing*, vol. 115, p. 108257, 2022.

[80] M. Aicardi, A. Bozzi, S. Graffione, R. Sacile, and E. Zero, "Alternating direction method of multipliers in distributed control of a system of systems: Application to a quadruple tank plant," *Control Engineering Practice*, vol. 149, p. 105972, 2024.